TEMPERATURE DISTRIBUTION OF ROUGH AIRLESS BODIES & VOLATILE STABILITY

L. RUBANENKO[1,2], O. AHARONSON[1], & N. SCHORGHOFER[3] [1]Weizmann Institute of Science, 234 Herzl St., Rehovot, Israel, 7610001, [2]UCLA, 595 Charles E Young Drive, LA, CA 90095 [3]Institute for Astronomy, University of Hawaii, 2680 Woodlawn Drive, Honolulu, HI 96822 (liorr@ucla.edu).

Introduction: Permanently shadowed regions (PSRs) on airless planetary bodies may harbor volatile deposits for periods comparable to the lifetime of bodies in the Solar System [1]. The prevalence of those cold-traps may be modeled by considering the effect of topography on the surface temperature distribution. Previous models have neglected scattering completely [2] or assumed a simplified scattering law with a pre-determined constant shadow temperature [3]. Others have simulated scattering using idealized shapes such as spherical craters [4-6]. More recent thermophysical models incorporate ray-surface intersection algorithms with subsurface heat conduction [7-10]**.** Differences between the simpler and the latter, more computationally demanding models appear when simulating temperatures at higher latitudes, where cold-traps may be stable. Here we develop and apply a thermophysical model to calculate the prevalence of cold-traps at high latitudes and review the effect of surface roughness on the stability of both surface and subsurface ice.

Model: Our model includes insolation, shadowing, infrared emission and multiple scattering from the surface, along with an implicit (unconditionally stable) algorithm to account for 1D subsurface conduction. We divide the topography into rectangular facets. Virtual light rays are cast as probes in all directions, and their intersection points with other objects are used in order to determine the objects' scale and distance from one another [11]. We account for the relative size and slope angles by considering the View Factor, a measure of the projected angular size of the facet as seen by the emitter. Subsurface conduction is modeled to a depth of several times the diurnal thermal skin depth. We validated our model by comparing its output to analytic results [2,5] and to Diviner measurements [12].

Spherical Craters: We employ our model using topography consisting of a single spherical crater with a depth-to-diameter ratio of 1/5, typical of impact craters on the Moon <15 km (Figure 1a). We vary the thermal inertia, I. We find that adding subsurface conduction alters the shadow temperature distribution of the crater as predicted in the past [5]. The peak temperature occurs after noon and for $I = 100\ \mathrm{J\,m^{-2}K^{-1}s^{-1/2}}$ is $\sim 20\ \mathrm{K}$ lower than the equilibrium in the most conductive case considered.

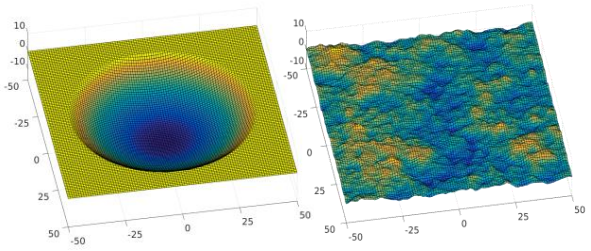

(a) (b)

Figure 1: Examples topographies used in the model. (a) A spherical crater. (b) Random topography with a Gaussian slope distribution.

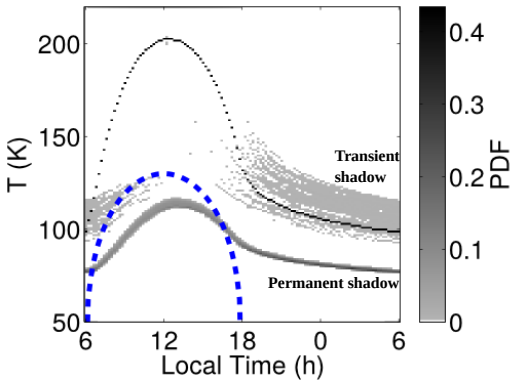

Figure 2: The time-dependent temperature distribution of a spherical crater with a depth-to-diameter ratio $1/5$, including conduction with $I = 100\ \mathrm{J\,m^{-2}K^{-1}s^{-1/2}}$. The dashed blue line shows the analytic solution for the shadow temperature (Ingersoll et al., 1992). The grey shading represents the PDF, the fractional area at a temperature-local time bin.

A notable feature of the temperature distribution is the doubly-peaked shadow temperature resulting from the heat conducted into the ground (Figure 2). This is ascribed to the two types of shadows found in a realistic crater: the permanent, colder shadow is an area that does not receive direct solar radiation throughout the diurnal cycle. The second type of shadow is a transient shadow, appearing in places briefly exposed to the Sun during the solar day. Therefore, the approximation of a uniform shadow temperature [4,5] fails when accounting for subsurface conduction; At every time step, transient shadows cover an area of 50%-60% of the total shadowed area, and are approximately $20\ \mathrm{K} - 40\ \mathrm{K}$ warmer than permanent shadows, meaning they radiate more flux. Thus, they are expected to contribute to the overall energy balance of the permanently shadowed facets and raise their temperature, an effect missing in an equilibrium models.

Stability of Surface Ice: The link between the temperature distribution and the surface roughness is used to estimate the prevalence of cold-traps on airless bodies. In order for an exposed surface to be considered a cold-trap, its temperature must not exceed 110 K – 120 K [1]. We therefore estimate the area fraction of a rough surface with low enough temperatures to harbor stable surface ice by applying our model to a rough random surface with a Gaussian slope distribution (Figure 1b) and identifying facets with $T_{\max} < 110$ K. Figure 3 shows the relation between the area fraction covered by cold-traps at different depths to the surface roughness. We find that, as expected, the area of cold-traps on rough surfaces grows with both latitude and roughness. We note that the dependence on latitude is such that the amount of stable ice increases by an order of magnitude between latitude 70° and 80°, from less that 1% in area fraction to several percent, in approximate agreement with Diviner estimates of surface temperatures at polar latitudes.

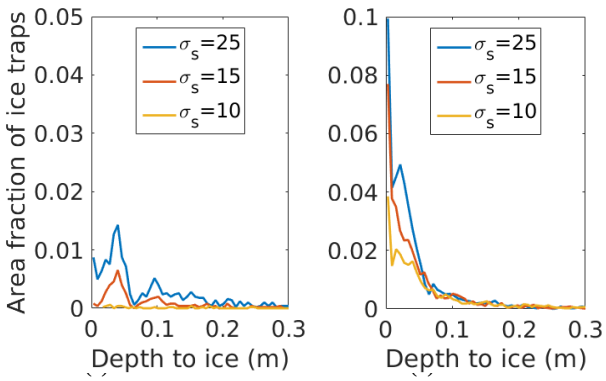

Figure 3: The depth to subsurface ice stability with $I = 25$ J m^{-2} K^{-1} s$^{-1/2}$. Topography does not affect ice stability beyond the skin depth, of order 10 cm.

Depth to ice: The temperature at which subsurface ice is stable is determined by the thickness of the overlying layer and its grain size [12,13]. We use this relation in order to find the necessary conditions for ice stability. Using our model, we find the temperatures of a conductive typical lunar subsurface and calculate the maximal diurnal temperature as a function of depth. This relation allows us to find the depth to ice stability, *i.e.* where the temperature curve intersects that predicted from Eq. 11 of [13]. With these assumptions, we find two regimes where stable subsurface ice is permitted: 1) ice may become stable within a few skin-depths of the surface, *i.e.* in the top decimeters. In this regime, stability is sensitively determined by the decay of the temperature oscillations. 2) At higher mean temperatures, ice is stable at much greater depths (not shown), where a substantial barrier to diffusion counteracts the loss rate. In this regime, the barrier thickness controls stability. For example, at a temperature of 135 K, a burial depth of ~120 m is required. We find that topography ceases to affect the depth to stable ice beyond the diurnal skin depth (~10 cm). Stability strongly depends on latitude, as even relatively rough surfaces ($\sigma_s = 15°$) have almost no stable ice at 70° latitude (Figure 3).

Slope Aspect of Stable Ice: Pole facing slopes provide more stable conditions for ice. We model the effect of surface roughness on this preference (Figure 4), and find rougher surfaces tend to show ice stability regions with a more uniform aspect distribution than flatter surfaces which harbor ice mostly on pole facing slopes. We attribute this difference to the fact that persistent shadows on smoother surfaces (lower RMS slope) are predominantly caused by self-shadowing of pole facing slopes, rather than mutual shadowing that occurs at arbitrary orientation.

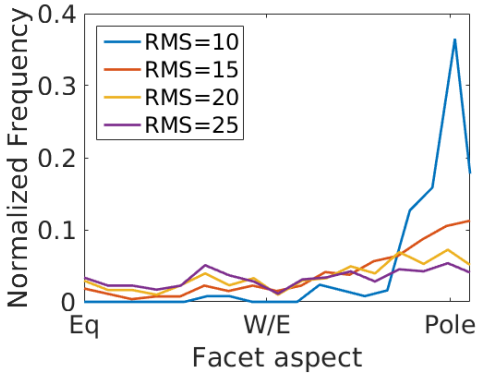

Figure 4: The normalized frequency of the slope aspect for cold traps (surfaces with temperature < 110 K). Flatter surfaces tend to have more ice on pole facing slopes, while rougher surfaces have a more uniform distribution of aspects where ice is stable.

References: [1] Watson, K, et al. (1961), *JGR*, *66*, 3033-3045. [2] Smith, B. G. (1967), *JGR*, *72*, 4059-4067. [3] Bandfield, J. L., et al. (2015), *Icarus 248*, 357-372. [4] Buhl, D., et al. (1968), *JGR*, *73*, 5281-5295. [5] Ingersoll, A. P., et al. (1992), *Icarus 100*, 40-47. [6] Hayne, P. O. and Aharonson, O. (2015), *JGR*, *120*, 1567-1584. [7] Paige, D.A., et al., *Science*, *258*, 643-646. [8] Vasavada A., et al. (1999), *Icarus*, *141*, 179-193. [9] Paige et al. (2009), *AGU*, Abstract #P31E-08. [10] Davidsson, B. J. R and Rickman, H. (2014), *Icarus*, *243*, 58-77. [11] Roth, S. D. (1982), *Comp. Graph. & Im. Proc.*, *18*, 109-144. [12] Paige, D. A. (2010), *Science*, *330*, 479-482. [13] Schorghofer, N. and Taylor, J. G. (2007), *JGR*, *112*, 1991-2012.